JRC TECHNICAL REPORTS

The energy dependence of fission-fragment characteristics for neutron-induced fission on Pu-239

Göök, A

Oberstedt, S.

2018

This publication is a Technical report by the Joint Research Centre (JRC), the European Commission's science and knowledge service. It aims to provide evidence-based scientific support to the European policymaking process. The scientific output expressed does not imply a policy position of the European Commission. Neither the European Commission nor any person acting on behalf of the Commission is responsible for the use that might be made of this publication.

Contact information
Name: Stephan OBERSTEDT
Email: stephan.oberstedt@ec.europa.eu
Tel.: +32 14 57 1361

Contents

Foreword

This report is the delivery 2018 of the work package 6410 FISSION Advanced studies of the nuclear fission process the Project ANDANTE and contributes to the Policy Area "Safe and secure use of nuclear energy"

Key orientation of the WPk 6410 is towards the enhanced safety of nuclear reactors and nuclear fuels through collecting, analysing and assessing the operational experience of nuclear power plants worldwide and disseminating information to the Member States' regulatory authorities.

The work summarized in the present report contributes to the research on the improvement of the safety assessments of innovative reactor designs in synergy with the Generation IV International Forum (GIF), the generation of reference scientific data on the safety performance and to the development of codes and models for safety assessment of both conventional and innovative nuclear fuels in operational, transient and accident conditions. It may help supporting the EU's internal policy on nuclear safety and the implementation of related EU directives and EU policy by providing state-of-the-art technical and scientific knowledge

Acknowledgements

Authors

Alf Göök, JRC – Directorate G – Unit G.2, alf.gook@ec.europa.eu

Stephan Oberstedt, JRC – Directorate G – Unit G.2, stephan.oberstedt@ec.europa.eu

Abstract

This report is in response to a nuclear data request on the OECD-NEA high priority request list for new measurements of prompt neutron multiplicities from ^{239}Pu(n,f) in the incident neutron energy range from thermal to 5 eV. There exists experimental evidence for strong fluctuations of the average neutron multiplicity from resonance to resonance in ^{239}Pu(n,f). These fluctuations have been shown to impact nuclear reactor benchmarks by reducing the criticality. One explanation for the fluctuating neutron multiplicity may be the competition between direct fission and the (n,γf) process. However, there is also evidence for fluctuations of the fission fragment mass yields from resonance to resonance. The mass yield fluctuations may also contribute to fluctuations of the neutron multiplicity averaged over all fission fragment masses. In order to model the contribution to the neutron multiplicity fluctuations by the fission fragment mass yield fluctuations new data on the correlations between fission fragment properties and neutron multiplicities are in need.

In this report we present an experiment carried out to determine prompt neutron multiplicity correlations with fission fragment masses and total kinetic energies. The experiment has been carried out at the GELINA facility at JRC-Geel. Correlations between average neutron multiplicities and fission fragment properties have been measured with improved resolution in both mass and TKE, compared to data from the literature. Results show that the dependence of average neutron multiplicity per fission and fission fragment mass split is weak.

1 Introduction

Fluctuations of the average prompt neutron multiplicity (nubar) from the reaction [239]Pu(n,f) in the incident neutron energy range of the resonances have been observed (Shackleton et al., 1973, Weston et al., 1974 and Gwin, 1984). In **Figure 1** experimental data and evaluations of these types of fluctuations in the incident neutron energy range below 120 eV are shown. Changes in nubar between 1-10% at the resonance energies are evident. The fluctuations have been shown to impact nuclear reactor benchmarks by reducing the criticality (Fort, 1988).

A new evaluation of the prompt fission neutron spectrum (PFNS) in the thermal energy range has determined a lower value of the average neutron energy than that reported in the existing evaluated nuclear data libraries (Pigni et al., 2017). The lower average neutron energy is in agreement with independent evaluations (Capote et al., 2016). A number of thermal-solution benchmarks have shown that the use of a softer prompt fission neutron spectrum at thermal energy, combined with new thermal neutron constants (adapted to fit with the IAEA standards), yields k-eff values that are larger than measurements by a margin that increases as the above-thermal-leakage fraction increases (De Saint Jean, 2014). Therefore a reduced criticality is needed for high-leakages solutions. Accordingly, the OECD-NEA high priority request list is asking for new measurements of nubar in [239]Pu(n,f), in the incident neutron energy range from thermal to 5 eV (Capote, 2018).

Figure 1. Fluctuations in the average neutron multiplicity as a function of the incident neutron energy in the [239]Pu(n,f) reaction.

Fluctuations of nubar in the region of the resonances is suspected to be due to competition between direct fission and the (n,γf) process, in which fission proceeds after the emission of a gamma-ray. The pre-scission gamma-ray caries away energy, as a consequence, the neutron multiplicity is lowered when the importance of the (n,γf) process is higher. For accurate evaluation of nubar it is, however, also necessary to
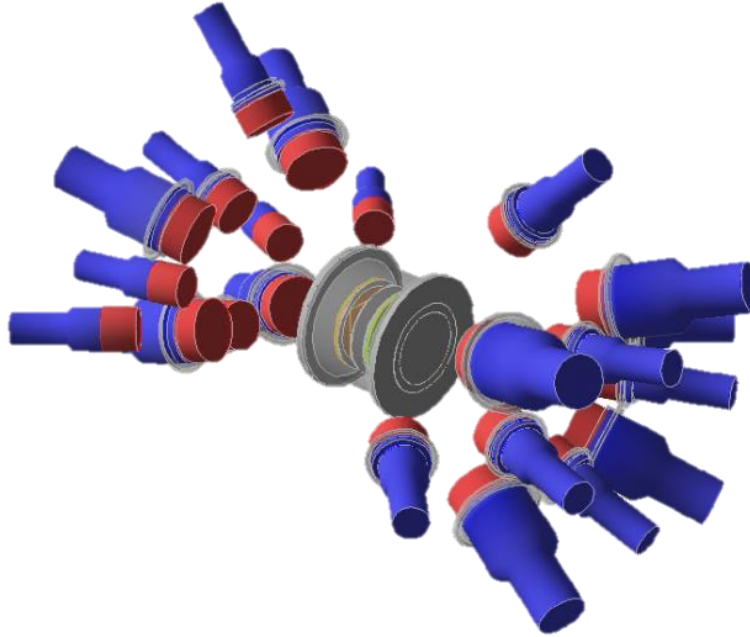
account for fluctuations of the fission fragment mass yields. In the present report we are presenting an experiment performed at the GELINA time of flight facility, where both the fission fragment mass yields as a function of the incident neutron energy and the dependence of nubar on the fission fragment mass has been studied. We are reporting here on the results of the correlation of the average number of emitted neutrons with the fission fragment mass and total kinetic energy (TKE) release. This data provide crucial input required to model the influence of mass yield fluctuations on nubar as a function of the incident neutron energy. The results on fission fragment mass yield fluctuations will be reported at a later time.

This report is also presenting plans to adapt the existing experimental setup, essential in order to meet the required accuracy on nubar in the incident neutron energy range from thermal to 5 eV.

2 Experiment

The experiment has been performed at the GELINA neutron time-of-flight facility at the JRC Geel site. The detector setup is located at the 10 m measurement station on flight-path 17. It is schematically illustrated in **Figure 1**, and consists of two parts: an array of proton recoil scintillators (SCINTIA) and a twin position-sensitive ionization chamber (2PIC) for fission fragments. More details about the detector setup are given in the following sub-sections of this report. The data acquisition is based on wave-form digitizers. A pulse from the common cathode of the 2PIC triggers the data acquisition to store digital wave forms from all ionization chamber electrodes and scintillation detectors on disk for offline analysis. Together with the wave-form data, 800 MHz time-stamp information is also written. The t_0-signal from the accelerator, generated just before an electron pulse hits the neutron producing target and a neutron pulse is produced, is used to reset the time stamp. This allows the incident neutron energy to be determined via the time-of-flight technique. The main experiment was performed with GELINA operating at 800 Hz repetition frequency. With the incident neutron flight-path length of 8.81 m, the lowest neutron energy accessible in this measurement is 0.26 eV. To avoid overlap of low energy neutrons from a former electron beam pulse, a Cd filter with an areal density of 0.7 g/cm^2 was placed in the beam.

Figure 2. Illustration of the experimental setup with the 2PIC in the centre surrounded by the 22 neutron detectors of the SCINTIA array. The GELINA neutron beam enters from the left and runs through the centre of the ionization chamber, perpendicular to the electrode plane.

2.1 Fission Fragment Detection

The 2PIC is used for determination of fission fragment masses and energies. The detector was developed at JRC-Geel and is described in detail elsewhere (Göök et al., 2016), some essential details will be repeated here. In principle, the detector is a twin Frisch gridded ionization chamber. However, the standard anode plates are replaced by position sensing readout electrodes. The fission target consists of a thin layer (29.95 µg/cm^2 Pu) of PuF$_4$ on a backing of gold covered polyimide. The fission target is placed in a hole in the common central cathode. The very thin target and backing allows for both of the fission fragments from a binary event to escape and ionize the gas on either side of the

6

cathode plate. Fission fragment energies and masses are determined via the double-kinetic-energy (2E) technique. For the purpose of calibration, we have used data collected with GELINA operating at 50 Hz repetition frequency. This allows the selection of thermal neutron induced fission in the time of flight spectrum, which has well known characteristics. During the 50 Hz run the Cd-filter was removed from the beam.

As counting gas pure CH_4 is used. The choice of this counting gas is motivated by its high drift velocity compared to the P-10 gas mixture, which is more commonly used with this detector. The high drift velocity helps reducing the effect of pile-ups present due to the high alpha activity of the ^{239}Pu target.

2.1.1 Determination of Mass and TKE

The masses $m_{1,2}^*$ and energies $E_{1,2}^*$ before neutron emission in a binary fission event are related via conservation of linear momentum, according to

$$m_{1,2}^* = m_{cn} \frac{E_{1,2}^*}{E_1^* + E_2^*},$$

where m_{cn} is the mass of the compound nucleus undergoing fission. Under the assumption of isotropic neutron emission from fully accelerated fragments, the energies before neutron emission $E_{1,2}^*$ are related to the energies after neutron emission $E_{1,2}$ by the approximation

$$E^* = E \frac{m^*}{m^* - \bar{v}(m^*, \text{TKE})},$$

where $\bar{v}$ is the number of neutrons emitted by the fragment. The dependence of $\bar{v}$ on mass and TKE can only be derived from the data once the 2E analysis is completed. As initial assumption we have used the evaluated data on $\bar{v}(m^*)$ from Wahl (1988) and the parametrization
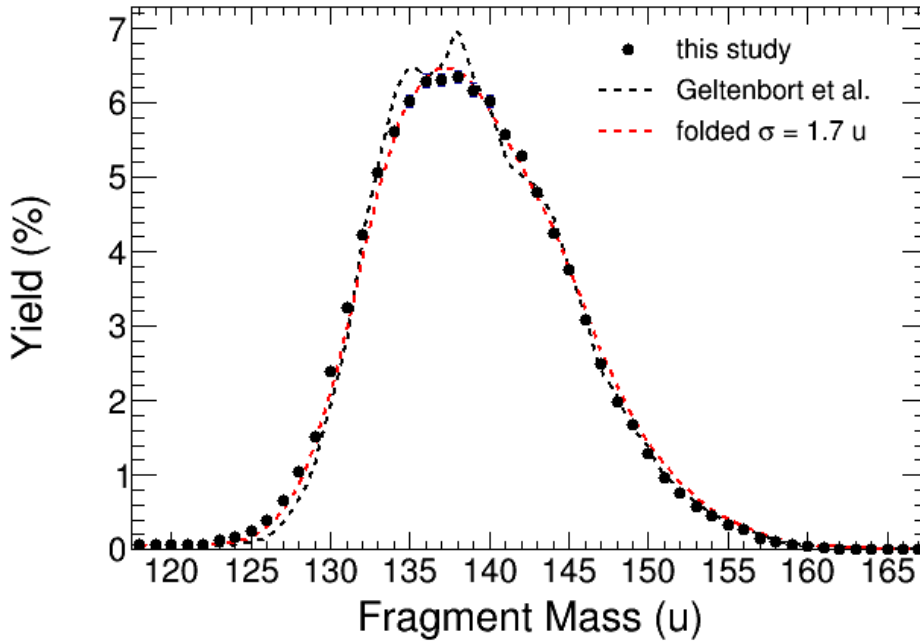
$$\bar{v}(m^*, \text{TKE})^* = \bar{v}(m^*) + \frac{\bar{v}(m^*)}{\bar{v}(m^*) + \bar{v}(m_{cn} - m^*)} \frac{\overline{TKE}(m^*) - TKE}{E_{sep}},$$

where E_{sep} = 8.6 MeV/n is the average energy necessary to emit a neutron (Nifenecker, 1973). The analysis was later repeated using the results for $\bar{v}(m^*)$ and E_{sep} = 8.51 MeV/n derived from the data. No significant changes in the results were observed between the two analyses; hence no further iteration was made. For the case when a neutron coincidence is required, an additional correction to the fragment energy according to Gavron (1974) is applied. The pulse height defect of the counting gas is corrected for as described by Hambsch et al. (1995), with parameters adjusted to reproduce known values of the average light and heavy fragment masses (Geltenbort et al, 1986) and TKE (Gönnenwein, 1991) from ^{239}Pu(n$_{th}$,f).

The intrinsic energy resolution of the ionization chamber is for fission fragments 0.6 MeV (Budtz-Jørgensen, 1987). However, the finite target thickness causes an uncertainty in the energy loss correction that dominates the resolution for the individual fragment, since the depth inside the target where the fission took place is unknown. This uncertainty is on average about 0.67 MeV, as determined from the observed energy loss in the target material. In addition to the resolution of the measured energies, conversion of the measured post-neutron energies to pre-neutron energies, relevant for calculating the fission fragment masses, adds broadening. The resolution due to neutron emission can be estimated according to Terrell (1962). Combined an average mass resolution of about 4-5 u (FWHM) is expected. The expectation is verified by comparing the mass distribution, selecting only thermal incident neutron energies from the present measurement, to high resolution double velocity data from Geltenbort et al. (1986), as displayed in Fig. 2. The red dashed line corresponds to the data of Geltenbort et al.

(1986) convoluted with a Gaussian resolution function; the best fit for the FWHM of this resolution function was found to be 3.9 u. Considering a mass resolution of 1-1.5 u (FWHM) for the double velocity experiment we arrive at a mass resolution around 4 u (FWHM).

Figure 3. Observed fission fragment mass distribution from ^{239}Pu(n_{th},f) compared to high resolution data from Geltenbort et al. (1986). The full red line corresponds to the data from Geltenbort et al. (1986) convoluted with a Gaussian resolution function with a FWHM of 3.9 u.

The resolution in TKE due to the target thickness was estimated to 0.1 MeV, based on energy loss calculations of typical fission fragments using TRIM (Ziegler, et al. 2008). This figure is significantly smaller than the resolution that applies to the individual fragments. This is because the uncertainty on the depth inside the target where the fission takes place cancels to a large extent. Due to the very thin target used in the present experiment the post-neutron TKE resolution is dominated by the intrinsic energy resolution of the ionization chamber and estimated to be 0.6 MeV.

The orientation of the fission axis is determined in the 2PIC from combined information on the electron drift time and charge division from the position sensitive electrodes. This gives the position of the centre of gravity of the charge distribution along the stopping tracks of both fission fragments individually. By connecting these two points by a straight line, the position of the fission event on the target plane as well as the orientation of the fission axis is extracted, with resolutions of 1.5 mm (FWHM) and 7° (FWHM), respectively. This information is then used to determine the relative orientation of the fission fragment velocity and the velocity of a neutron detected in any of the scintillators. A more detailed account of this analysis has been published earlier (Göök et al., 2016). The 2PIC covers nearly 4π of the solid angle. However, due to energy straggling and uncertainty in the energy loss corrections, fission fragment masses cannot be accurately determined for angles of emission larger than 60◦ with respect to the target normal. The collimation is done during the offline data analysis by imposing a cutoff angle using the information extracted on the fission axis orientation. The cutoff angle causes a fission fragment efficiency that varies as a function of angle relative to a specific neutron detector ϑ_L. By counting the number of fissions as a function of ϑ_L (regardless of whether a neutron has been registered in coincidence or not) the fission fragment efficiencies are determined and accounted for; cf. Göök et al. (2016).

2.2 Prompt Neutron Detection

Prompt fission neutrons (PFN) were detected in an array of proton recoil scintillators. The array is illustrated in **Figure 2**. In Table 1 the neutron detector array is summarized. The table includes properties of the neutron detectors and their position relative to the centre of the fission target inside the ionization chamber.

Table 1 Summary of the neutron detector array. Three different type of detectors were used; the EJ-301 is an NE-213 equivalent liquid scintillator, while the paratherphenyl (pth) and the stilbene are organic crystal scintillators. The distance from the centre of the ^{239}Pu target to the centre of the individual detector is denoted by d. The detector orientation axis is given by the polar θ_d and azimuthal φ_d angles with respect to the incident beam direction. The position of the individual detector was determined with an accuracy of 0.2 mm, using a measuring arm (ROMER Absolute Arm 7530, Hexagon Metrology). The last column gives the size of the scintillator.

Type	d (cm)	θ_d (deg.)	φ_d (deg.)	diameter x height (cm x cm)
stilbene	43.37	134.47	−177.16	8.00×5.00
pth	41.04	161.88	−174.20	8.00×5.00
pth	41.24	159.78	−4.41	8.00×5.00
pth	41.83	133.69	−3.30	8.00×5.00
EJ-301	45.65	129.35	88.01	10.16×5.10
EJ-301	43.58	161.73	84.27	10.16×5.10
EJ-301	43.58	160.96	−86.74	10.16×5.10
EJ-301	47.98	47.89	93.09	10.16×5.10
EJ-301	43.79	44.86	179.37	10.16×5.10
EJ-301	43.32	17.26	177.89	10.16×5.10
EJ-301	42.5	16.48	−97.41	10.16×5.10
EJ-301	44.93	16.9	100.25	10.16×5.10
EJ-301	45.9	18.17	0.18	10.16×5.10
EJ-301	45.46	41.74	−1.46	10.16×5.10
EJ-301	44.82	151.34	38.79	12.70×5.10
EJ-301	46.42	154.85	140.9	12.70×5.10
EJ-301	45.37	151.54	−129.30	12.70×5.10
EJ-301	45.25	149.55	−50.51	12.70×5.10
EJ-301	45.89	27.48	137.85	12.70×5.10
EJ-301	44.68	28.14	−136.51	12.70×5.10
EJ-301	45.47	24.78	−48.97	12.70×5.10
EJ-301	44.06	26.29	45.6	12.70×5.10

For the purpose of studying correlations between neutrons and fission fragments it is necessary to know the neutron detection efficiency as a function of the energy of the prompt neutrons. In order to determine this, a dedicated measurement with a ^{252}Cf source placed inside the ionization chamber was performed. The prompt fission neutron spectrum (PFNS) emitted in the spontaneous fission decay of ^{252}Cf is known with an accuracy of about 1-3% in the energy range 0.15 to 11 MeV, and is considered as a neutron standard. Hence, by forming the ratio of observed and evaluated (ENDF/B.VII-1) PFNS for this decay the neutron detection efficiency can be determined. The ^{252}Cf source was deposited on a thin (220 μg/cm^2) Ni foil, and had an activity of about 3300 fissions/s. The ^{252}Cf measurement was performed under the same experimental conditions as the ^{239}Pu(n,f) measurement, except for the incident neutron beam which was not present. When determining the PFNS no selection of fission fragment emission angle is made. In fact, for this purpose only the signal from the 2PIC's central cathode is used as a fission trigger, with a threshold adjusted to discriminate against α-decay. The very thin targets used for the measurements and the large solid angle of acceptance of the fission fragment detector ensures that the PFNS is unperturbed by this selection.

The PFN energy is determined from the flight time of the neutrons from the ionization chamber to the scintillation detector, according to

$$E = m_0 c^2 (\gamma - 1), \tag{4}$$

where $m_0 c^2 = 939.565$ MeV is the rest energy of the neutron and γ is the Lorentz factor, given by

$$\gamma = \left(1 - \left(\frac{l}{tc}\right)^2\right)^{-1/2}. \tag{5}$$

In Eq (5) l is the flight-path length, t is the flight time and c is the speed of light in vacuum.
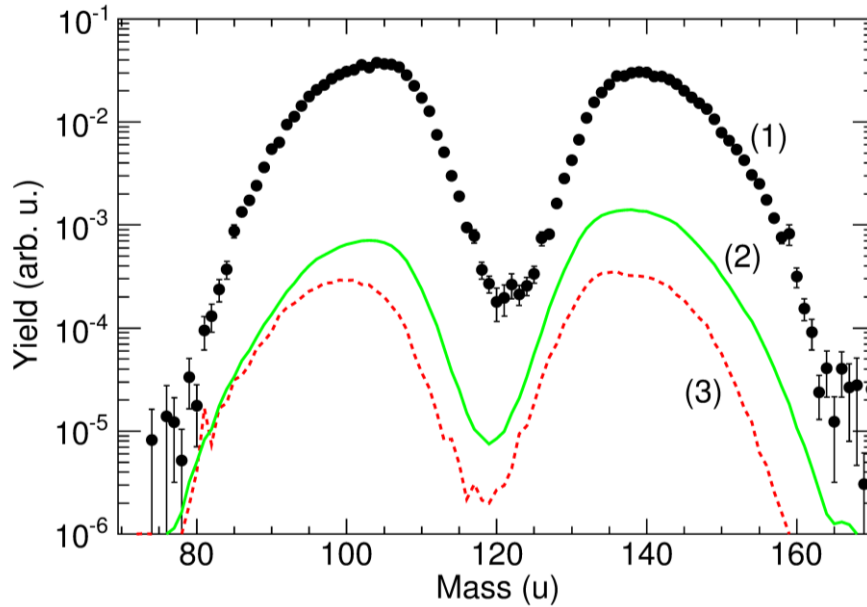
The energy resolution is given by the combination of uncertainty in the flight time and the flight-path length, due to the size of the detectors (as given in Table I). The combined timing resolution of the ionization chamber and the scintillation detectors is dominated by the ionization chamber, and has been determined to be 1.1 ns (FWHM). The selection of prompt fission neutrons is made using pulse-shape discrimination (PSD) and pulse-height thresholds. In addition to neutrons, fission is accompanied by prompt γ-ray emission. For low energy deposits in the scintillators, PSD fails to distinguish between γ-rays and neutrons, leaving a residual γ-ray component. Most of the prompt γ emission happens at the instant of fission and up to a few ns later. Within the same time range, high-energy neutrons, which are emitted with a very low intensity, will arrive in the detectors. Therefore, the very high-energy region of the neutron spectrum is most sensitive to false events induced by γ-rays. In order to reduce the effect of such false events, the pulse-height threshold is made to depend on the time of flight. The rate of background events caused by interactions of the neutron beam with the experimental environment, as well as ambient background, was determined by counting, as a function of the pulse height threshold, the number of accidental coincidences before the prompt γ-ray peak, in the time-of-flight interval [−500,−10] ns.

2.3 Analysis of Fission Fragment and Prompt Neutron Coincidences

A neutron detected in coincidence with fission may originate from either of the two fragments. However, due to the kinematic boost, the probability that the detected neutron originates from the fragment detected in the same hemisphere as where the neutron detector is located is much higher (Budtz-Jørgensen, 1987). The data analysis is

first made assuming that the probability to detect a neutron from the complementary fragment is zero. With the kinematic information (neutron energy, fission fragment energy and mass, as well as the angle between neutron and fragment velocities) obtained in the laboratory reference frame, the kinematics in the c.m. frame can be reconstructed. Once the neutron spectrum in the c.m. frame has been obtained the contribution from the complementary fragment may be estimated and subtracted. The data analysis procedure has been developed and applied in our earlier works (Göök et al., 2014 and Göök et al., 2018) and is described in more detail there. In the present experiment, as well as in our earlier work (Göök et al., 2018) on ^{235}U(n,f) we did allow for the spectral shape to depend on the mass number of the primary fragment. The effect of ambient background events on each of the observables, presented in section 3, was estimated in a Monte Carlo like fashion, using the fission fragment data without requiring coincidence with the neutron detectors. For each fission event, a false coincidence is generated by randomizing a time of flight, and giving it a weight according to the determined background intensity. The event is then propagated through the analysis as if it were a real event, so that all the same selection criteria are applied. Finally, for each measured distribution a background distribution is obtained that is subtracted from the measured one. The magnitudes of these corrections are shown as a function of fragment mass in **Figure 4**. The black points are the efficiency corrected number of recorded neutron coincidences per fission event; the full green line is the background due to accidental coincidences, while the dashed red line is the number of neutrons from the complementary fragment. The correction due to complementary fragment neutrons is small, and for most masses negligible. The correction is smaller than 1% over the whole mass range except around 130 u where it reaches a maximum of around 5%. The larger of the two corrections is due to the accidental coincidences with ambient background. The magnitude of this correction is 3.5% of the total number of recorded coincidences. At masses around 80 u and 130 u, where the number of emitted neutrons is small, it reaches about 10% and 15%, respectively.

Figure 4. Fission neutron yield and background components versus fragment mass. The black points (1) represent the measured yield, background due to accidental coincidences is represented by the full green line (2), and the dashed red line (3) represents the neutron yield from the complementary fragment.
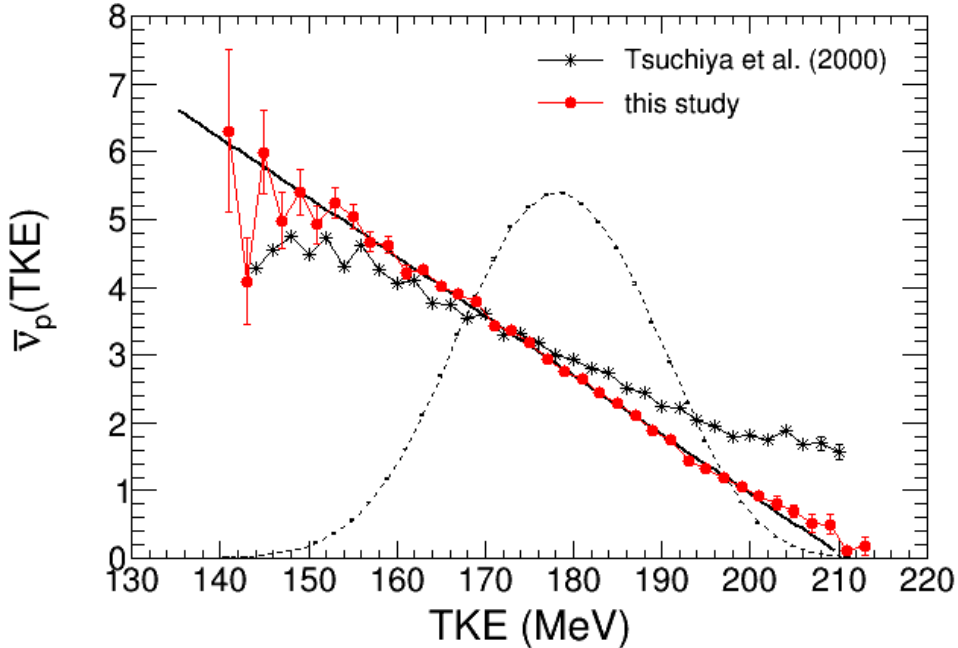
3 Experimental Results and Discussion

In this section results on the correlations of nubar with properties of the fission fragment is presented. The present results are compared to data from earlier experiments at thermal incident neutron energies. In the present experiment the average neutron multiplicity correlations have been measured with unprecedented resolution in both mass and TKE, compared to earlier data.

In **Figure 5** the average neutron multiplicity per fission as a function of TKE is compared to data from Tsuchiya et al. (2000). As expected from energy balance considerations, a close-to-linear decrease of $\bar{v}$ with increasing TKE is observed. A weighted least-square fit results in an inverse slope $-\partial \text{TKE}/\partial_v = 11.4$ MeV/n. This value is close to the value observed by us in the spontaneous fission of ^{252}Cf (Göök et al, 2014), as well as in ^{235}U(n,f) (Göök et al, 2018). It is clear, from a visual inspection of **Figure 5** that the present data are in disagreement with the data of Tsuchiya et al. (2000). We have observed similar discrepancies with earlier experiments for the reaction ^{235}U(n,f) (Göök et al., 2018). As described in (Göök et al., 2018) those discrepancies are explained by better resolution in TKE in our experiment. The same arguments presented for ^{235}U(n,f) apply also to the present experiment.

Figure 5. Average prompt neutron multiplicity per fission as a function of the fragment TKE. Data obtained in this study is compared to data from literature. The dotted black line shows the shape of the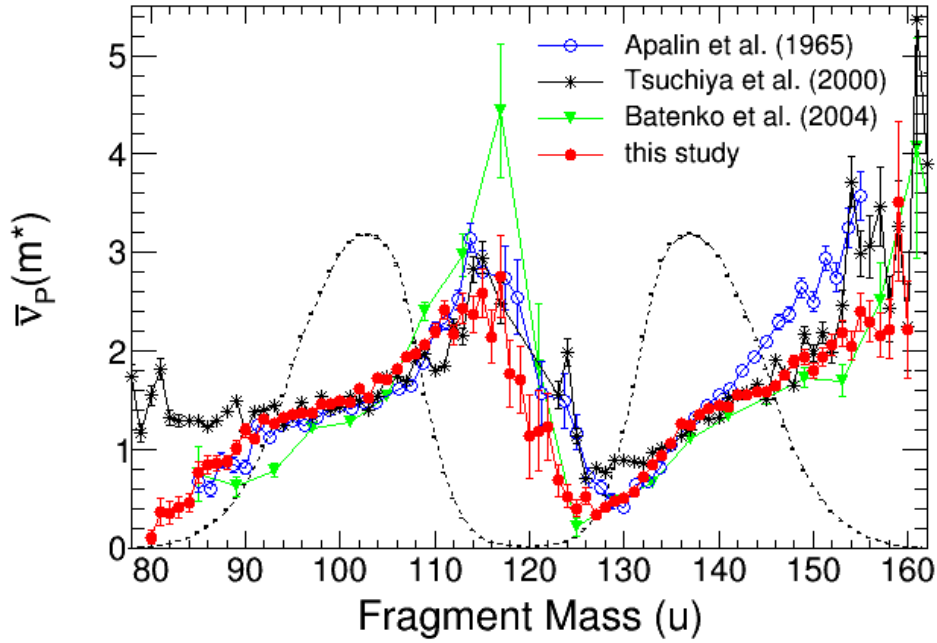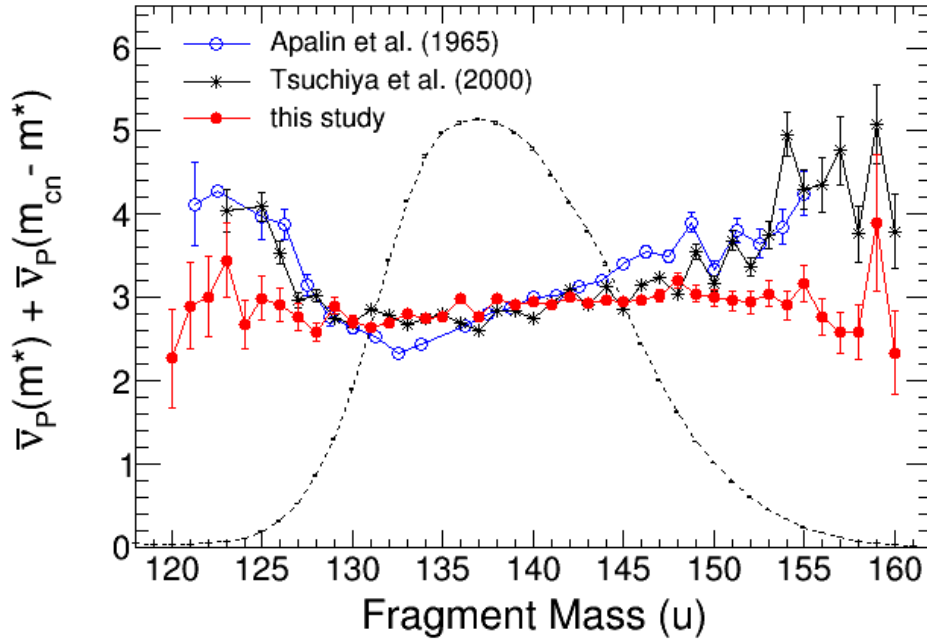 fission fragment TKE distribution (without absolute scale). The full black line represent a least square fit of a straight line to the data from this study with an inverse slope $-\partial \text{TKE}/\partial_v = 11.4$ MeV/n.

In **Figure 6** and **Figure 7** data from the present experiment on the dependence of prompt neutron multiplicity on fission fragment mass is shown and compared to data from literature. The neutron multiplicity per fission fragment is shown in **Figure 6**, the present results show good agreement with data from Tsuchiya et al. (2000) and Batenko et al. (2004), in the region around the asymmetric mass peaks. In the region of symmetric mass split the present data shows a lower neutron multiplicity than the earlier

experiments. The data of Tsuchiya et al. (2004) shows less pronounced minima in the sawtooth like curve (around fragment masses of 80 u and 130 u). This could be related to the approximately 50% poorer mass resolution in their experiment (6 u).

Pronounced (Hambsch, 1989) and slightly weaker (Hambsch, 2010) incident neutron-energy dependent fluctuations of the fission fragment mass yields have been found in resonance-neutron induced fission on ^{235}U and ^{239}Pu, respectively. This would influence the average neutron multiplicity, if the fragement-mass dependence of the same was also strong (Hambsch, 1989). This dependence, obtained by summing the multiplicity of light and heavy fragment, is shown in **Figure 7**. In contrast to earlier experimental results (Apalin et al., 1965 and Tsuchiya et al., 2000) the present study show a much flatter behaviour as a function of fragment mass. The difference with respect to the data of Apalin et al. (1965) can be understood in terms of a missing correction in the data analysis. Namely, the effect of the recoil of the emitted neutrons on the fission fragment mass determination. This effect was first discussed by Gavron (1974), i.e. years after the experimental data of Apalin et al (1965) was published. Hence, we may assume that Apalin et al. have not accounted for this effect. The recoil effect shows up in experimental data as an increase in neutron multiplicity for the heaviest fragments in the mass yield distribution, as well as around the symmetric mass split (Gavron, 1974). Consequently, the dependence of the total number of neutrons per fission will show an increased slope as a function of the heavy fragment mass as well as a large increase around symmetric mass splits.

Figure 6. Average prompt neutron multiplicity per fragment as a function of the fission fragment mass. Data obtained in this study is compared to data from literature. The dotted black line shows the shape of the fission fragment mass distribution (without absolute scale).

Figure 7. Average prompt neutron multiplicity per fission as a function of the heavy fission fragment mass. Data obtained in this study is compared to data from literature. The dotted black line shows the shape of the fission fragment mass distribution (without absolute scale).

The total number of prompt neutrons per fission does not show a strong dependence on fission fragment mass. Therefore, we may rule out fission fragment mass yield

15

fluctuation as a major contribution to nubar fluctuations observed in resonance neutron induced fission on ^{239}Pu. The more prominent contribution should be due to the competition between the direct (n,f) and the (n,γf) processes. Minor contribution of the fragment mass yield fluctuations can be estimated using the data presented in **Figure 7** and data on the fragment mass yields as a function of the incident neutron energy. The energy dependent fragment mass yields are currently under evaluation and will be presented at a later stage.

4 Conclusions and Outlook

We have reported on measurements of the average neutron multiplicity correlations with fission fragment mass and TKE in ^{239}Pu(n,f). The correlations have been measured with improved resolution in both mass and TKE, compared to data from the literature. The new data provide crucial input required to model the influence of mass yield fluctuations on nubar as a function of the incident neutron energy.

In order to reach the target statistical accuracy on nubar, below about 1% at the resonances (Capote, 2018), the present experimental setup must be modified. Based on the results presented in section 3 we may rule out fission fragment mass yield fluctuations as a major contribution to the fluctuations of nubar as a function of incident neutron energy. Therefore, the updated experimental setup will focus on measurement of the neutron multiplicity as a function of incident neutron energy alone. That is, the experiment will not attempt to measure the correlation between neutron multiplicity and fission fragment masses. This greatly simplifies the requirements on the fission fragment detector and allows us to construct a detector whose sole task is to identify when fission takes place. The foreseen detector is a parallel plate ionization chamber with 12 layers of ^{239}Pu. The targets are currently under production. Each target will have an areal density of around 120 µg/cm^2. This leads to an increase in the expected fission rate in the experiment by a factor of 48, compared to the experiment described in section 2.

Recently, Lynn et al. (2018) published a list of resonance which are the most likely candidates to exhibit an observable (n,γf) effect, based on their theoretical calculations. For these resonances the expected statistical uncertainty after half a year of measurement at GELINA has been estimated, as listed in **Table 2**. The estimation is based on the number of prompt fission neutrons observed in the experiment described in section 3, and the increase in fission rate with the modified setup. For most of the candidate resonances the expected statistical uncertainty is well below the expected fluctuation of nubar which lies between 5-10 %. The candidates for observing the (n,γf) effect all have small fission cross sections. In the incident neutron energy region below 5 eV the fission cross section is much larger, hence the expected statistical accuracy is well below 1% there.

In order to measure nubar in the energy range below 0.3 eV a dedicated run with GELINA operating at 50 Hz repetition frequency will be necessary.

Table 2 Parameters for resonances that appear below 100 eV in the n + ^{239}Pu reactions, which are the most likely candidates to exhibit an observable (n,γf) effect, according to Lynn et al. (2018). The last column lists the expected statistical uncertainty on nubar for the updated setup after half a year of measurement at GELINA.

E_{res} (eV)	Γ_f (meV)	Expected stat. unc. (%)
27.29	2.8	5.0
35.49	3.5	2.3
41.46	6.4	0.9
44.53	4.4	0.9
50.14	5.0	0.6
82.77	5.2	1.1

References

Apalin, V.F., et al., *Nucl. Phys.* 71, 553 (1965).

Batenko, O.A., et al., *AIP Conf. Proc.*, 769, 1003 (2004).

Budtz-Jørgensen, C., et al., *Nucl. Instrum. Methods Phys. Res.*, Sect. A 258, 209 (1987).

Capote, R. , et at., *Nucl. Data Sheets*, 110, 1 (2016).

Capote., R., *NEA Nuclear Data High Priority Request List – 99H*, url: https://www.oecd-nea.org/dbdata/hprl/hprlview.pl?ID=520 (2018).

De Saint Jean, C., (coordinator), *Co-ordinated Evaluation of Plutonium-239 in the Resonance Region, Nuclear Energy Agency*, International Evaluation Cooperation, NEA/WPEC-34, Report NEA/NSC/WPEC/DOC(2014), pp. 447 (2014).

Fort, E., et al., Nucl. Sci. And Eng., 99, 375 (1988).

Gavron, A., *Nucl. Instrum. Methods* 115, 99 (1974).

Geltenbort, P., et al., *Radiat. Eff.* 93, 57 (1986).

Gönnenwein, F., in *The Nuclear Fission Process*, edited by C. Wagemans (CRC, Boca Raton, FL), Chap. 8, pp. 287–473 (1991).

Göök, A., et al., *Nucl. Instrum. Methods Phys. Res.*, Sect. A 830, 366 (2016).

Göök, A., et al., *Phys. Rev. C* 90, 064611 (2014).

Göök, A., et al., Phys. Rev. C 98, 044615 (2018).

Gwin, R., et al., *Nucl. Sci. and Eng.*, 87, 381 (1984).

Hambsch, F.-J., et al., *Nucl. Instrum. Methods Phys. Res*., Sect. A 361, 257 (1995).

Hambsch, F.-J., et al., *Nucl. Phys. A*, 491, 56 (1989).

Hambsch, F.-J., et al., *Proceedings of the Scientific Workshop on Nuclear Fission Dynamics and the Emission of prompt Neutrons and gamma Rays*, EUR 24802, Publications Office of the European Union, Luxembourg, 2011, doi:10.2787/4298.

Lynn, J.E., et al., Phys. Rev. C, 97, 064601 (2018).

Nifenecker, H. et al., in *Proceedings of the Third IAEA Symposium on the Physics and Chemistry of Fission* (IAEA, Vienna), Vol. 2, p. 117 (1973).

Pigni, M.T., et al., 'n+235U resonance parameters and neutron multiplicities in the energy region below 100 eV', *EPJ Web of Conferences*, 146, 02011 (2017).

Shackleton, D., et al., *Phys. Lett.*, 18, 31 (1965).

Terrell, J., *Phys. Rev.* 127, 880 (1962).

Tsuchiya, C., et al., *Jour. of Nucl. Sci. Tech.*, 37, 941, (2000).

Wahl, C., *At. Data Nucl. Data Tables* 39, 56 (1988).

Weston, L.W., et al.,*Phys. Rev. C*, 10, 1402 (1974).

Ziegler, J., et al., SRIM computer code, version 2008.04.

List of abbreviations and definitions

nubar   average prompt neutron multiplicity

PFNS   prompt fission neutron spectrum

TKE   total kinetic energy

2PIC   twin position-sensitive ionization chamber

FWHM   Full width at half maximum

PFN   prompt fission neutron

2E   double kinetic energy

List of figures

List of tables

The European Commission's science and knowledge service

Joint Research Centre

JRC Mission

As the science and knowledge service of the European Commission, the Joint Research Centre's mission is to support EU policies with independent evidence throughout the whole policy cycle.

EU Science Hub
ec.europa.eu/jrc

@EU_ScienceHub

EU Science Hub – Joint Research Centre

Joint Research Centre

EU Science Hub

Publications Office